Theor Chem Acc (2011) 128:579–592
DOI 10.1007/s00214-010-0824-5

REGULAR ARTICLE

The reaction between HO and $(H_2O)_n$ (n = 1, 3) clusters: reaction mechanisms and tunneling effects

Javier Gonzalez · Marc Caballero · Antoni Aguilar-Mogas · Miquel Torrent-Sucarrat · Ramon Crehuet · Albert Solé · Xavier Giménez · Santiago Olivella · Josep M. Bofill · Josep M. Anglada

Received: 5 July 2010 / Accepted: 13 September 2010 / Published online: 30 September 2010

Abstract The reaction between the HO radical and $(H_2O)n$ (n = 1, 3) clusters has been investigated employing high-level quantum mechanical calculations using DFT-BH&HLYP, QCISD, and CCSD(T) theoretical approaches in connection with the 6-311 + G(2df,2p), aug-cc-pVTZ, and aug-cc-pVQZ basis sets. The rate constants have also been calculated and the tunneling effects have been studied by means of time–dependent wavepacket calculations, performed using the Quantum–Reaction Path Hamiltonian method. According to the findings of previously reported theoretical works, the reaction between HO and H_2O begins with the formation of a pre-reactive complex that is formed before the transition state, the formation of a post-reactive complex, and the release of the products. The reaction between HO and $(H_2O)_2$ also begins with the formation of a pre-reactive complex, which dissociates into H_2O…HO + H_2O. The reaction between HO and $(H_2O)_3$ is much more complex. The hydroxyl radical adds to the water trimer, and then it occurs a geometrical rearrangement in the pre-reactive hydrogen-bonded complex region, before the transition state. The reaction between hydroxyl radical and water trimer is computed to be much faster than the reaction between hydroxyl radical and a single water molecule, and, in both cases, the tunneling effects are very important mainly at low temperatures. A prediction of the atmospheric concentration of the hydrogen-bonded complexes studied in this work is also reported.

Keywords Atmospheric chemistry · Hydroxyl radical · Water clusters · Reaction mechanism · Tunneling effects

Published as part of the special issue celebrating theoretical and computational chemistry in Spain.

J. Gonzalez · M. Torrent-Sucarrat · R. Crehuet · S. Olivella · J. M. Anglada (✉)
Departament de Química Biològica i Modelització Molecular, Institut de Química Avançada de Catalunya, IQAC–CSIC, c/Jordi Girona, 18, 08034 Barcelona, Spain
e-mail: anglada@iqac.csic.es

M. Caballero · A. Aguilar-Mogas · A. Solé · X. Giménez
Departament de Química Física, Universitat de Barcelona, c/Martí i Franqués, 1, 08028 Barcelona, Spain

J. M. Bofill (✉)
Departament de Química Orgànica, Universitat de Barcelona, c/Martí i Franqués, 1, 08028 Barcelona, Spain
e-mail: jmbofill@ub.edu

M. Caballero · A. Aguilar-Mogas · A. Solé · X. Giménez · J. M. Bofill
Institut de Química Teòrica i Computacional, Universitat de Barcelona (IQTCUB), c/Martí i Franquès, 1, 08028 Barcelona, Spain

1 Introduction

Hydroxyl radical (HO) is a very important species in several fields of chemistry. In the earth atmosphere, it plays a central role in the degradation processes of air pollutants such as carbon monoxide or volatile organic compounds (VOCs) [1]. In atmospheric conditions with low NO_x concentrations, hydroxyl radical can destroy one ozone molecule producing molecular oxygen and hydroperoxyl radical, which destroys a second ozone molecule yielding molecular oxygen and recycling the hydroxyl radical [1–6]. Moreover, it also interacts with atmospheric gas-phase water, and it can be taken up by atmospheric aerosols or water droplets, so that it can oxidize soluble tropospheric pollutants [7–9]. In biological systems, hydroxyl radical is also a powerful oxidant. It is one of the well-known

"reactive oxygen species", which play an important role in oxidative stress, aging, and cell damage [10–13]. In environmental chemistry, hydroxyl radical is a highly oxidant molecule reacting by addition to double bonds or by abstracting hydrogen atoms. Its chemistry is directly related to waste water treatments, and it is associated with the peroxone chemistry as one of the advanced oxidation processes [14–17].

$$H_2O + HO \rightleftharpoons HO + H_2O \quad (1)$$

Among the reactions involving hydroxyl radical, the reaction with water (reaction 1) has become a prototype for the hydrogen atom abstraction reactions by free radicals. This reaction is also relevant for atmospheric purposes because it can be associated with the isotopic composition of the atmospheric water [18]. In the troposphere, the concentration of hydroxyl radical is close to 10^{-7} molecule cm^{-3} [3], and a typical gas-phase concentration of H_2O is 6.95×10^{17} molecule cm^{-3}, corresponding to 50% of relative humidity at 298 K, so reaction 1 can easily take place. Unfortunately, the direct measurement of the rate constant of reaction 1 is not possible because it is a silent reaction regarding the formation of the products. However, Dubey et al. [18] investigated the deuterium-labeled reactions, and they suggested an activation energy $E_a = 4.2 \pm 0.5$ kcal mol^{-1} over the temperature range 300–420 K. Several theoretical studies have also been published in the literature regarding reaction 1 [18–25], reporting an energy of activation close to 10 kcal mol^{-1}, but pointing out an important contribution from quantum mechanical tunneling effect.

In the present work, we are considering the theoretical study of reaction 1 along with reactions of hydroxyl radical with a cluster of two and three water molecules. Our aim is twofold: (a) Firstly, to investigate how additional water molecules affect reaction 1. It has been recently shown in the literature that water vapor produces a catalytic effect in several reactions of atmospheric relevance [26–34], and therefore it is relevant to have a deeper knowledge of the role that water vapor plays in gas-phase reactions involving hydrogen atom abstraction processes; (b) Secondly, to analyze the quantum chemical tunneling effect in the studied reactions and consequently its influence on the reaction rate. In this regard, it is known that complex structures involving hydrogen transfer processes might lead to enhanced tunneling [35–37]. In addition, it is worth noting that water clusters exhibit a network of hydrogen bonds, whose continuous rearrangement is inherently of quantum mechanical origin. Zero-point energy issues add to the former phenomena, thereby restricting the available energy flows and substantially altering the ensuing H-atom motion, when compared to classical mechanics predictions [38]. Therefore, this quantum effect is studied here with emphasis on multidimensional issues and, in particular, on specificities involving water clusters of increasing size, by means of an efficient quantum reaction path methodology.

As far as we know, there are no data yet in the literature regarding the reaction between hydroxyl radical and the water dimer and trimer, despite its potential importance in the chemistry of the troposphere and in climate change. Pfeilsticker and coworkers [39] detected water dimers in the atmosphere by near-infrared absorption spectroscopy, and they suggested an atmospheric concentration of 6×10^{14} molecule cm^{-3} at 292 K; Dunn et al. [40] predict a dimer concentration of 9×10^{14} molecule cm^{-3} and Goldman et al. [41] predict concentrations up to 1.7×10^{15} molecule cm^{-3} at high relative humidity. In these studies, it has also been speculated that water trimers may also exist in the troposphere, with a predicted concentration of 2.6×10^{12} molecule cm^{-3}. Overall, these data stress the potential role that water dimer and trimer can play in the atmosphere.

2 Technical details of the calculations

We employed density functional BH&HLYP method [42] with the 6–311 + G(2df,2p) basis set [43, 44] to optimize all stationary points investigated in this work. At this level of theory, we also computed the harmonic vibrational frequencies to verify the nature of the corresponding stationary points (minimum or saddle point) and to provide the zero-point vibrational energy (ZPE) and the thermal contributions to the enthalpy and Gibbs energy. Moreover, we performed intrinsic reaction coordinate calculations (IRC) [45–48] to ensure that the transition states connect the desired reactants and products. More accurate relative energies have been obtained by performing single-point CCSD(T) [49–52] energy calculations at the optimized geometries using the more flexible aug-cc-pVTZ basis set [53, 54].

The reliability of our results has been checked by performing two additional sets of calculations on the water dimer and trimer as well as on the prototype reaction 1. The first one involves single-point CCSD(T) energy calculations using the aug-cc-pVQZ basis set at the BH&HLYP optimized geometries. The second one, involves re-optimization of some selected stationary points employing the QCISD method [55] with the 6-311 + G(2df,2p) basis set and then carrying out single-point CCSD(T) energy calculations at the optimized geometries using the aug-cc-pVTZ basis set. In this case, we checked that the harmonic vibrational frequencies obtained at QCISD and BH&HLYP levels of theory compare well, which is necessary for the study of the tunneling effects.

Moreover, for reaction 1, we also carried out additional CASSCF calculations [56] to investigate the possibility of finding valley-ridge inflection (VRI) points along the potential energy surface (PES). In this case, we employed the 6-311 + G(2df,2p) basis set and an active space consisting in three electrons and three orbitals. Furthermore, to get a reliable energy position of the VRI point, we performed single-point energy calculations at the CCSD(T) level of theory with the aug-cc-pVTZ basis set for the transition state and the VRI point located at the CASSCF level of theory.

All the DFT, QCISD, and CCSD(T) calculations have been performed by using the Gaussian 03 suite of programs [57], whereas the CASSCF calculations have been done using the GAMESS program [58].

The tunneling dynamics have been studied by means of time-dependent wavepacket calculations, performed using our recently developed Quantum–Reaction Path Hamiltonian method (Q–RPH) [59]. A coherent state wavepacket is propagated in time along a potential energy profile, obtained from the IRC associated with each of the present reactions, under a position-dependent mass term, which accounts for the effect of the transversal vibrational modes. It is thus an effective one-dimensional reaction–path implementation of the nuclear dynamics [60]. Thanks to the reduced-dimensional nature of the method, it favorably scales with an increase in the number of degrees of freedom, being suitable for multidimensional dynamics studies of large polyatomic systems [61, 62], including quantum effects. The variable mass term is found to depend on gradients and hessians along the reaction path, so that it is fully computed prior to the propagation step and stored along with the potential energy profile [63]. The Q–RPH method has proven to reliably describe the multidimensional dynamics of several polyatomic reactions such as $H + H_2$ and, remarkably, $F + H_2$ (including the low-energy resonances), by means of the above effective one-dimensional, variable mass method. The transmission factor, i.e., the Fourier transform of a suitable wavepacket's autocorrelation function, has been used to provide quantitative estimations of the tunneling effect. Calculations are made defining a sufficiently large spatial grid and then obtaining the time evolution with small time increments, by means of an Askar–Cakmak numerical method [64]. The number of grid points and the time increment are used as convergence parameters to ensure stability of results.

3 Results

As usual in many reactions of atmospheric interest, all reactions investigated in this work begin with the formation of hydrogen-bonded complexes occurring before the transition states, the formation of post-reactive hydrogen-bonded complexes, and the release of products. Moreover, all reactions considered in this work are symmetric, so that pre-reactive and post-reactive complexes are the same species and the reactants and products too. In what follows the pre-reactive complexes are labeled by the prefix **CR** followed by a number and the transition states are labeled by the prefix **TS** followed by a number too. In many cases, it occurs that there are isomers of a given stationary point that differ in the relative orientation of dangling hydrogen atoms. To distinguish between these isomers, we appended lower case letters to the acronym of the corresponding stationary point.

3.1 The water dimer and trimer

The water dimer and trimer have already been reported in the literature, and we considered them as reactants in the present study. The results regarding their relative stabilities are contained in Table 1, whereas Fig. 1 shows the most relevant geometrical parameters. As shown in Table 1 we checked the reliability of our calculations by performing geometry optimizations at the BH&HLYP and QCISD levels of theory, and the computed bond lengths obtained using both methods differ in less than 0.03 Å. At the optimized geometries, we carried out single-point energy calculations at the CCSD(T) level of theory with the aug-cc-pVTZ and aug-cc-pVQZ basis sets for de dimer and with the aug-cc-pVTZ for the trimer.

The water dimer $(H_2O)_2$ has C_S symmetry. Its electronic state is X^1A', and we computed a binding energy of 2.86 kcal mol^{-1} in an excellent agreement with the 3.3 kcal mol^{-1} reported in the literature [40, 65].

The water trimer has two isomers having a three-membered ring structure, and we labeled them as $(H_2O)_3$-a and $(H_2O)_3$-b. Both differ in the orientation of the dangling hydrogen atoms (two toward one side and the third toward the opposite side in $(H_2O)_3$-a; and the three pointing to the same side in $(H_2O)_3$-b, see Fig. 1). The probability that the water trimer is formed by a collision of three water molecules is very low, and therefore we assumed that it is formed by reaction between a water dimer and a water molecule. Thus, taking $(H_2O)_2 + H_2O$ as reactants, the computed binding energies are 7.73 and 7.40 kcal mol^{-1} for $(H_2O)_3$-a and $(H_2O)_3$-b, respectively, which compares very well with the 7.26 kcal mol^{-1} reported in the literature [40].

3.2 The reaction between hydroxyl radical and a single water molecule

As pointed out previously, there are several theoretical studies in the literature dealing with this reaction [18, 19, 21–24]. Therefore, we considered only the reaction path

Table 1 Zero-point energies (ZPE in kcal mol^{-1}), entropies (S in a.u.), and relative energies, ZPE-corrected energies, enthalpies, and Gibbs energies (in kcal mol^{-1}) for the formation of the water dimer and trimer

Compound	Method[a]	ZPE	S	ΔE	Δ(E + ZPE)	ΔH(298 K)	ΔG(298 K)
$H_2O + H_2O$	A	27.88	90.0	0.00	0.00	0.00	0.00
	B	27.27	90.1	0.00	0.00	0.00	0.00
	C	27.27	90.1	0.00	0.00	0.00	0.00
$(H_2O)_2$	A	30.10	69.4	−5.23	−3.01	−3.52	2.62
	B	29.50	69.7	−5.20	−2.97	−3.45	2.63
	C	20.59	69.7	−5.09	−2.86	−3.34	2.75
$(H_2O)_2 + H_2O$	A	44.05	114.4	0.00	0.00	0.00	0.00
	B	44.05	114.4	0.00	0.00	0.00	0.00
$(H_2O)_3$-a	A	47.38	80.0	−11.07	−7.73	−9.00	1.24
	B	47.38	80.0	−11.00	−7.67	−8.93	1.31
$(H_2O)_3$-b	A	46.88	83.8	−10.24	−7.40	−8.34	0.77
	B	46.88	83.8	−10.19	−7.36	−8.29	0.82

[a] Method A stands for values computed at the CCSD(T)/aug-cc-pVTZ//BH&HLYP/6-311 + G(2df,2p) level with ZPE, enthalpy, and Gibbs energy corrections obtained at the BH&HLYP/6-311 + G(2df,2p) level; Method B stands for values computed at the CCSD(T)/aug-cc-pVTZ//QCISD/6-311 + G(2df,2p) level with ZPE, enthalpy, and Gibbs energy corrections obtained at the QCISD/6-311 + G(2df,2p) level; Method C stands for values computed at the CCSD(T)/aug-cc-pVQZ//QCISD/6-311 + G(2df,2p) level with ZPE, enthalpy, and Gibbs energy corrections obtained at BH&HLYP/6-311 + G(2df,2p) level

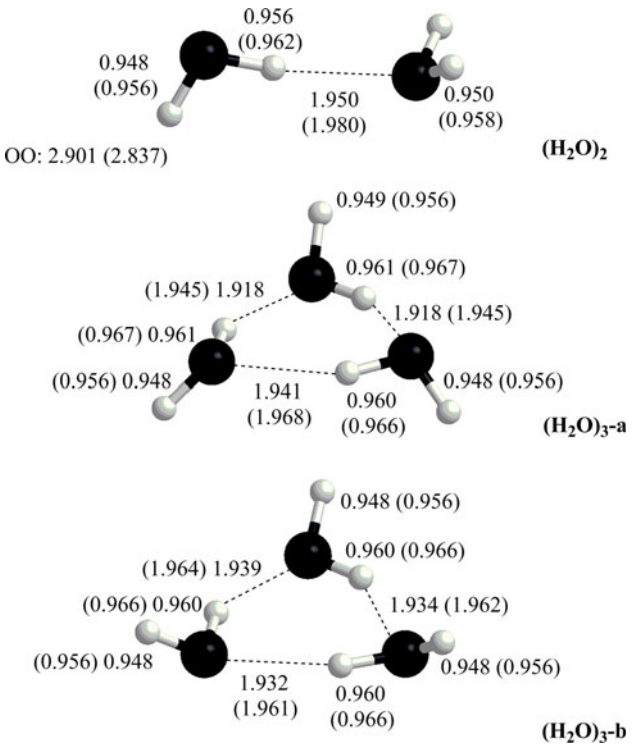

Fig. 1 Selected geometrical parameters obtained at BH&HLYP and QCISD levels of theory for the optimized structures of water dimer and trimer. Values in parenthesis correspond to QCISD-optimized geometries

having the lowest energy barrier, and we will focus on the main trends regarding the reaction mechanism. For this reaction, we also checked the reliability of our calculations by performing geometry optimizations at BH&HLYP and QCISD levels of theory, and the computed bond lengths obtained using both methods differ in less than 0.04 Å. At the optimized geometries, we carried out single-point energy calculations at the CCSD(T) level of theory with the aug-cc-pVTZ and aug-cc-pVQZ basis sets.

Table 2 contains the relative energies of reaction 1, and Fig. 2 shows an energy profile along with the most relevant geometrical parameters of the stationary points. The reaction begins with the barrierless formation of a pre-reactive hydrogen-bonded complex (**CR1**), occurring before the transition state (**TS1**), followed by the formation of a post-reactive hydrogen-bonded complex (**CR1**) and the release of the products. **CR1** has C_S symmetry (X^2A'), and it is formed by interaction between the hydrogen of the hydroxyl radical and the oxygen of water. The computed hydrogen bond length is 1.898 Å, and its binding energy is computed to be 3.78 kcal mol^{-1}. Our results are in excellent agreement with other experimental and theoretical results from the literature [27, 66–71]. **TS1** has C_2 symmetry (^2B), and it involves a hydrogen atom transfer (HAT) mechanism. The hydrogen atom being transferred is placed midway between the two oxygen atoms ($d_{OH} = 1.150$ Å). The process corresponds to the homolytic breaking and forming of the OH bonds, and it involves an adiabatic energy barrier of 12.53 kcal mol^{-1}, relative to **CR1**, which is in good agreement with other results from the literature [19, 21, 22, 24]. Table 2 shows that the energy barrier computed at different levels of theory used in this work differs in less than 0.26 kcal mol^{-1}. This provides further support to the reliability of our results.

Table 2 Zero-point energies (ZPE in kcal mol^{-1}), entropies (S in a.u.), and relative energies, ZPE-corrected energies, enthalpies, and Gibbs energies (in kcal mol^{-1}) for the reaction between HO and H_2O

Compound	Method[a]	ZPE	S	ΔE	Δ(E + ZPE)	ΔH(298 K)	ΔG(298 K)
HO + H_2O	A	19.5	87.5	0.00	0.00	0.00	0.00
	B	19.0	87.6	0.00	0.00	0.00	0.00
	C	19.5	87.5	0.00	0.00	0.00	0.00
CR1	A	21.5	67.3	−5.90	−3.85	−4.49	1.54
	B	21.2	67.0	−5.87	−3.72	−4.39	1.77
	C	21.5	67.3	−5.83	−3.78	−4.42	1.61
TS1	A	18.8	60.2	9.27	8.55	7.00	15.14
	B	18.4	60.3	9.15	8.56	7.02	15.17
	C	18.8	60.2	9.48	8.75	7.21	15.35

[a] Method A stands for values computed at the CCSD(T)/aug-cc-pVTZ//BH&HLYP/6-311 + G(2df,2p) level with ZPE, enthalpy, and Gibbs energy corrections obtained at the BH&HLYP/6-311 + G(2df,2p); Method B stands for values computed at the CCSD(T)/aug-cc-pVTZ//QCISD/6-311 + G(2df,2p) level with ZPE, enthalpy, and Gibbs energy corrections obtained at the QCISD/6-311 + G(2df,2p); Method C stands for values computed at the CCSD(T)/aug-cc-pVQZ//BH&HLYP/6-311 + G(2df,2p) level with ZPE, enthalpy, and Gibbs energy corrections obtained at the BH&HLYP/6-311 + G(2df,2p)

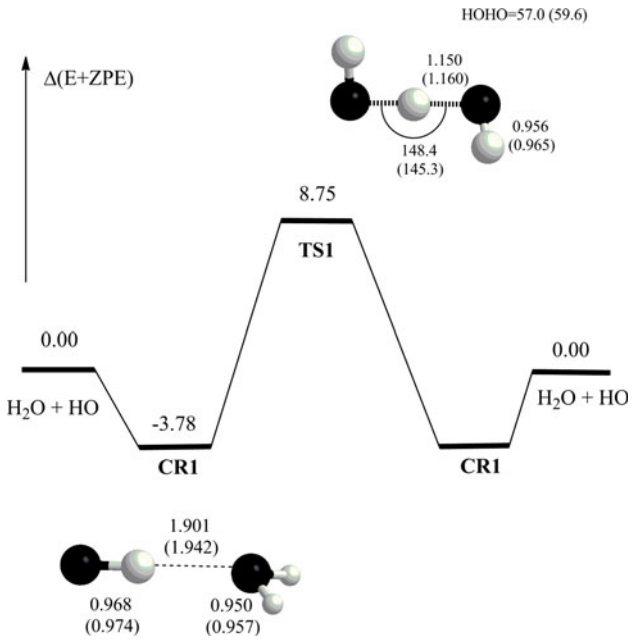

Fig. 2 Schematic reaction profile and selected geometrical parameters, at BH&HLYP and QCISD levels of theory, for the stationary points of the H_2O + HO reaction. Values in parenthesis correspond to QCISD-optimized geometries

With respect to the PES of the HO + H_2O reaction, there is a controversy in the literature regarding the features of the pre-reactive hydrogen-bonded complex. Unresolved question concerns whether the pre-reactive complex is the HOH…OH species, as suggested by Hand et al. [22], or the global minimum H_2O…HO (**CR1**), as pointed out by Masgrau et al. [19] and by Uchimaru et al. [21]. To bring more light to this point, we also considered the possibility that along the PES, it could exist a branching of the reaction that could occur through a VRI point [72]. We note that the steepest descent from the transition state in mass-weighted Cartesian coordinates is the simplest and widely used representation of a reaction path, which is well known as the IRC [48]. However, it should be taken into account that the IRC does not bifurcate, and due to this fact this representation of a reaction path is not well adapted to tackle the problem of branching reaction paths. Nevertheless, the VRI points gain importance when tackling the problem of reaction path branching. In fact, the possible existence of a VRI point along the PES in many cases explains the mixture of products observed experimentally, and now it is considered in many mechanistic studies [73]. From strictly theoretical point of view, the VRI points may form a manifold in the configuration space of the chemical species. This manifold can have the dimension $N-2$, if the configuration space of the PES has dimension N [74]. The characteristic attribute of a VRI point is that at least an eigenpair of the Hessian at this point has zero eigenvalue. This eigenvalue changes its sign when going along the gradient, where the corresponding eigenvector is orthogonal to the gradient. This means that a valley changes into a ridge or vice versa. The above two conditions, namely eigenvalue zero and zero overlap between the corresponding eigenvector with the gradient, characterize the $N-2$ dimensional manifold. In addition to the VRI points another possibility emerges, that is, the IRC meets in a point a direction with zero curvature of the PES orthogonal to the gradient. There, the gradient is not orthogonal to one of the eigenvectors of the PES, in the general case, the eigenvalues are not zero. The zero curvature of the PES along the level line comes from a suitable linear combination of the eigenvectors. This point is labeled as valley-ridge transition point (VRTp). Notice that the features of a

VRI point are stronger than those of a VRTp point. As will see below, the present PES possesses this type of point.

In the PES associated with the present reaction mechanism, the IRC curve leads directly from the transition state **TS1** to the corresponding deeper valley. The IRC curve does not follow the crest of the ridge that leads to another transition state, and it leads to one minimum that corresponds to the global H_2O…HO (**CR1**) minimum. In other words, the located IRC leaves the asymmetric ridge, and it goes to a minimum. However, this IRC path crosses an equipotential line or contour line of the PES with null curvature and meets with the border of the ridge region. At the CASSCF level of theory, the VRTp is characterized by a HO…HOH length of 1.458 Å and a HO…H–OH angle of 151 degrees. Taking into account the CCSD(T) energies computed at the CASSCF geometries, we predict that the VRTp is located at 3.99 kcal mol^{-1} below **TS1**. The border of the ridge region is defined by the set of points such that the projected Hessian matrix $[(\mathbf{I} - \mathbf{P}^T)\ \mathbf{H}\ (\mathbf{I} - \mathbf{P})$, where the **P** matrix is build by the gradient direction and the six zeros corresponding to translations and rotations] has eigenvectors with null eigenvalues in addition to these seven mentioned directions. These eigenvectors with null eigenvalues are orthogonal to the gradient vector. Notice that these eigenvectors are not eigenvectors of the full Hessian matrix. At each point of the border line of the ridge region, the direction of the equipotential line has null curvature, and this direction is a linear combination of a subset of eigenvectors of the full Hessian matrix. The existence of a VRTp has important implications since both the HOH…OH complex and the global minimum H_2O…HO (**CR1**) can be reached through this reaction.

3.3 The reaction between hydroxyl radical and a water dimer

Figure 3 displays a schematic representation of the energy profile of the reaction, along with the most relevant geometrical parameters of the corresponding stationary points. Table 3 contains their relative energies. For each of the stationary points, we found two isomers differing in the relative orientations of the dangling hydrogen atoms. These two isomers are distinguished from each other by appending the letter a, and the results displayed in Table 3 show that the two isomers of each stationary point are almost energetically degenerate. For the sake of clarity, we have drawn in Fig. 3 only one of these two isomers for each stationary point, and the discussion along the text will refer to only one of these isomers.

The potential energy profile schematized in Fig. 3 shows that, starting at the $(H_2O)_2$ + HO reactants, the reaction begins with the formation of a hydrogen bond complex **CR2**, for which we computed a binding energy of 7.42 kcal mol^{-1}. This complex has a three-membered ring structure where the two water molecules and the hydroxyl radical are held together by three hydrogen bonds. The calculated geometrical parameters compare quite well with those reported recently by Tsuji et al. [75]. Then, the reaction can proceed in two different ways, namely (a) dissociating into the H_2O…HO hydrogen bond complex plus H_2O and (b) proceeding through three different transition states. In this case, the exit channels are the same species than in the reactant channels.

Regarding to path (a), the **CR2a** complex has a geometric orientation that allows to dissociate directly into

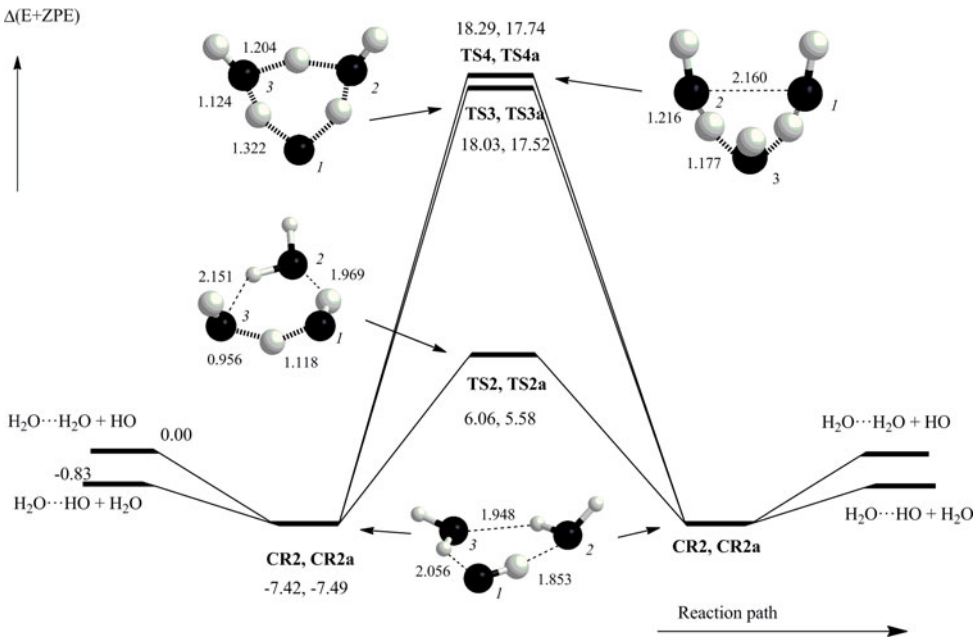

Fig. 3 Schematic reaction profile and selected geometrical parameters, at BH&HLYP level of theory, of the stationary points of the $(H_2O)_2$ + HO reaction

Table 3 Zero-point energies (ZPE in kcal mol^{-1}), entropies (S in a.u.), and relative energies, ZPE-corrected energies, enthalpies, and Gibbs energies (in kcal mol^{-1}) for the reaction between HO and $(H_2O)_2$

Compound	ZPE	S	ΔE	Δ(E + ZPE)	ΔH(298 K)	ΔG(298 K)
$H_2O\ldots H_2O + OH$	35.7	111.9	0.00	0.00	0.00	0.00
$H_2O\ldots HO + H_2O$	35.5	112.3	−0.66	−0.83	−0.96	−1.07
CR2	38.5	79.7	−10.28	−7.42	−8.67	0.93
CR2a	38.1	77.9	−9.94	−7.49	−9.03	1.12
TS2	35.5	76.2	6.27	6.06	4.28	14.95
TS2a	35.4	76.7	5.85	5.58	3.86	14.36
TS3	34.8	66.9	18.86	18.03	14.90	28.31
TS3a	34.7	67.0	18.45	17.52	14.41	27.80
TS4	36.2	67.7	17.79	18.29	15.38	28.55
TS4a	35.8	68.2	17.60	17.74	14.90	27.94

Values computed at the CCSD(T)/aug-cc-pVTZ//BH&HLYP/6-311 + G(2df,2p) level with ZPE, enthalpy, and Gibbs energy corrections obtained at the BH&HLYP/6-311 + G(2df,2p)

$H_2O\ldots HO + H_2O$ products, and the computed reaction energy is −0.83 kcal mol^{-1}. This process is tagged in the present work as reaction 2, and it is very important from atmospheric purposes as it contributes to the formation of the hydrated hydroxyl radical in the atmosphere.

$$(H_2O)_2 + HO \rightarrow \mathbf{CR2a} \rightarrow H_2O\ldots HO + H_2O \qquad (2)$$

Regarding to path (b), we found three different elementary reactions. The first one occurs through **TS2a**, which has a three-membered ring structure. This reaction involves the homolitic breaking and forming of the O*3*–H and H–O*1* bonds, respectively, so that the hydroxyl radical abstracts one hydrogen atom from a water molecule through a HAT mechanism. Figure 3 shows that the hydrogen atom being transferred is slightly closer (0.956 Å) to the oxygen atom of the water moiety than to the oxygen atom of the radical (1.118 Å) and that the transition state is stabilized by two hydrogen bonds. From an energetic point of view, our calculations predict this transition state to lie 5.58 kcal mol^{-1} above the energy of the reactants water dimer plus hydroxyl radical (see Table 3). At this point, it is worth comparing this value with the 8.75 kcal mol^{-1} computed for the transition state of the $H_2O + HO$ reaction described in the previous section (see Table 2). Consequently, the addition of a second water molecule produces a relative energy stabilization of the transition state of 3.17 kcal mol^{-1}, which can be attributed to the energy stabilization produced by the formation of two hydrogen bonds in **TS2a**. However, looking at the energy barrier relative to the **CR2a** complex, the computed value is 13.07 kcal mol^{-1}, which is even slightly larger than that reported for the naked reaction (12.40 kcal mol^{-1}, see Table 2). Consequently, it seems that the possible catalytic effect originated by the hydrogen bond stabilizations occurring in the transition state is counteracted by the enhanced stability of the pre-reactive complex, in a similar way as reported by Allodi et al. [70] for the methane oxidation by hydroxyl radical.

The second and third elementary reactions occur through **TS3** and **TS4**, which lie very high in energy (about 18 kcal mol^{-1} above the energy of the $(H_2O)_2 + HO$ reactants; see Table 3; Fig. 3), so that it is expected that they do not play any role. However, these elementary reactions are interesting from a mechanistic point of view. The analysis of **TS3** wave function indicates that the unpaired electron is mainly located over the hydroxyl radical moiety. It does not participate at all in the process, and the reaction mechanism involves a *triple proton transfer process*. In **TS4**, the different atoms are oriented in such a way that the unpaired electron of the hydroxyl radical moiety interacts with one oxygen atom of a water molecule, so that it occurs a transfer of an electron from this oxygen atom (O*2*) to the oxygen of the hydroxyl radical (O*1*), and this originates a simultaneous transfer of two protons (from O*2* to O*3* and from O*3* to O*1*, see Fig. 3). This elementary reaction corresponds to a *proton coupled electron transfer mechanism* (pcet), and similar processes have been described recently in the literature for the gas-phase oxidation of formic acid by hydroxyl radical and for the same process assisted by a single water molecule [25, 27, 76].

3.4 The reaction between hydroxyl radical and water trimer

Figure 4 contains a schematic energy profile of the reaction between $(H_2O)_3$ and HO radical, along with the most relevant geometrical parameters of the main stationary points. Table 4 contains the relative energies. Figure 4 shows that the reaction begins with the formation of a complex between the water trimer and the hydroxyl radical (**CR3**), with a computed binding energy of 4.45 kcal mol^{-1}. This complex retains the three-membered ring structure of the

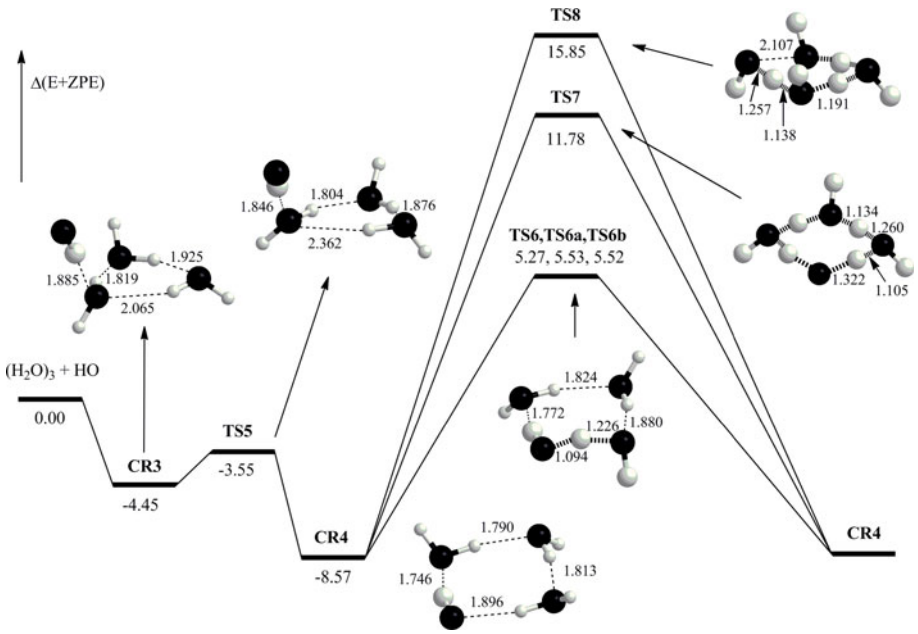

Fig. 4 Schematic reaction profile and selected geometrical parameters, at BH&HLYP level of theory, of the stationary points of the $(H_2O)_3$ + HO reaction. The reaction products are the same species than the reactants, and therefore they are not explicitly drawn

Table 4 Zero-point energies (ZPE in kcal mol^{-1}), entropies (S in a.u.), and relative energies, ZPE-corrected energies, enthalpies, and Gibbs energies (in kcal mol^{-1}) for the reaction between HO and $(H_2O)_3$

Compound	ZPE	S	ΔE	Δ(E + ZPE)	ΔH(298 K)	ΔG(298 K)
$(H_2O)_3$ + OH	52.9	122.6	0.00	0.00	0.00	0.00
$(H_2O)_2$…HO + H_2O	52.5	124.7	4.71	4.23	4.25	3.61
CR3[a]	54.8	99.3	−6.27	−4.45	−4.86	2.07
TS5[a]	53.9	99.9	−4.55	−3.55	−4.03	2.74
CR4	55.3	93.4	−10.91	−8.57	−9.42	−0.72
TS6	52.3	89.2	5.90	5.27	3.87	13.82
TS6a	52.1	90.4	6.38	5.53	4.24	13.83
TS6b	52.2	89.8	6.25	5.52	4.18	13.94
TS7	50.1	78.4	14.63	11.78	8.86	22.03
TS8	51.3	78.6	17.45	15.85	13.04	26.14

Values computed at the CCSD(T)/aug-cc-pVTZ//BH&HLYP/6-311 + G(2df,2p) level with ZPE, enthalpy and Gibbs energy corrections obtained at the BH&HLYP/6-311 + G(2df,2p)

[a] For the enthalpic, and Gibbs energy corrections, see Footnote 1

water trimer, and the hydrogen atom of the radical interacts with one of the oxygen atoms of $(H_2O)_3$ cluster. As in the previous section, for each stationary point there are three isomers differing in the relative orientations of the dangling hydrogen. They are almost degenerate in energy and, for the sake of clarity, we will consider the lowest energy one along the discussion.

The reaction goes on through **TS5**[1] to form the **CR4** complex, which has a four-membered ring structure (see Fig. 4). It is stabilized by four hydrogen bonds, and it lies 8.57 kcal mol^{-1} below the sum of the energies of the water trimer and the hydroxyl radical reactants. Our computed geometrical parameters compare quite well with those reported recently by Tsuji et al. [75]. After this complex, the reaction can proceed through three different reaction paths. The three elementary reactions have the same electronic features as described in the previous section for the reaction of the water dimer with the hydroxyl radical, and they will be not discussed here. The first reaction (HAT process) goes through **TS6,** and it involves the homolytic breaking and forming of the O*4*-H and H-O*1* bonds, respectively. Our calculations predict this transition state to lie 5.27 kcal mol^{-1} above the reactants energy, and the computed energy barrier is 13.84 kcal mol^{-1} relative to **CR4**. As discussed in the previous section, **TS6** lies lower in energy, relative to the separate reactants, than **TS1** of the

[1] The CR3 → CR4 path is very flat and we have failed to find TS5 at BH&HLYP level of theory We have optimized it, and CR3 too, using the B3LYP functional and their corresponding ZPE, entropy and enthalpy corrections have been employed in this case.

naked reaction, due to the extra stabilization originated by the hydrogen bond interactions. However, the energy barrier is also slightly larger because of the stability of the pre-reactive complex, counteracting, in part, thus the possible catalytic effect.

The transition structure of the second reaction path (**TS7**) lies 11.78 kcal mol^{-1} above the energy of the reactants, and the process involves the simultaneous transfer of four protons. The third reaction path goes through **TS8,** and it lies 15.85 kcal mol^{-1} above the energy of the reactants. In the same way as discussed for **TS5** above, this process involves the transfer of an electron from oxygen atom (O*4*) to the oxygen of the hydroxyl radical (O*1*), and this originates a simultaneous transfer of three protons (from O*2* to O*1*, from O*3* to O*2,* and from O*4* to O*3*), through proton-coupled electron transfer mechanism. The large energy barrier computed for these processes suggests that they will not play any role in the chemistry of the atmosphere.

3.5 Tropospheric concentration of the $(H_2O)_2$, $(H_2O)_3$, H_2O…HO, $(H_2O)_2$…HO, and $(H_2O)_3$…HO complexes

The calculations carried out in this work allow us to obtain the equilibrium constants for the formation of the water adducts reported in this work. With these values, we can estimate the atmospheric concentration of water dimer and trimer and the adducts formed between these complexes and the hydroxyl radical. This information is very interesting for atmospheric purposes, and therefore we considered three different conditions of relative humidity, namely 25, 50, and 75%, and temperatures ranging between 278 and 308 K. Reactions 3–8 have been considered for estimating the concentration of these species and, for the complexes containing hydroxyl radical, we considered a HO concentration of 1.0×10^7 molecules cm^{-3}.

$$H_2O + H_2O \rightleftharpoons (H_2O)_2 \quad (3)$$

$$(H_2O)_2 + H_2O \rightleftharpoons (H_2O)_3\text{-a} \quad (4)$$

$$(H_2O)_2 + H_2O \rightleftharpoons (H_2O)_3\text{-b} \quad (5)$$

$$HO + HO \rightleftharpoons H_2O\ldots HO(\mathbf{CR1}) \quad (6)$$

$$(H_2O)_2 + HO \rightleftharpoons (H_2O)_2\ldots HO(\mathbf{CR2}) \quad (7)$$

$$(H_2O)_3\text{-b} + HO \rightleftharpoons (H_2O)_3\ldots HO(\mathbf{CR4}) \quad (8)$$

In Table 5, we collected the computed equilibrium constants of these reactions, and Table 6 contains the estimated concentration of the $(H_2O)_2$, $(H_2O)_3$, H_2O…HO, $(H_2O)_2$…HO, and $(H_2O)_3$…HO complexes. Our calculations predict that the dimer concentration ranges between 5.95×10^{13} and 1.06×10^{16} molecule cm^{-3}, whereas the trimer concentration ranges between $1.59 \cdot 10^{12}$ and 1.21×10^{15} molecule cm^{-3}. These values compare with the estimated values between 6 and 9×10^{14} molecule cm^{-3} for the dimer [39, 40] although Goldman et al. predict higher concentrations, up to 1.7×10^{15} molecule cm^{-3}, at higher relative humidity [41].

Regarding the concentrations of the $(H_2O)_n$…HO complexes, the results displayed in Table 6 show that our calculations predict atmospheric concentrations of H_2O…HO in the 1.01×10^4–8.78×10^4 molecule cm^{-3} range, whereas the concentrations of the $(H_2O)_2$…HO and $(H_2O)_3$…HO complexes are predicted to be much smaller, up to 1.14×10^3 molecule cm^{-3}. For the H_2O…HO, our results compare very well with the 5.5×10^4 molecule cm^{-3} predicted by Allodi et al. at 298 K [70] but for the $(H_2O)_2$…HO and $(H_2O)_3$…HO complexes our calculations differ in about one order of magnitude from those predicted by Allodi et al. In analyzing these values, it should be pointed out that they have been obtained considering a population of the hydroxyl radical of 10^7 molecule cm^{-3}, and therefore predicted concentration of these complexes will increase several orders of magnitude if local conditions imply higher concentrations of hydroxyl radical.

3.6 Tunneling dynamics and rate constants

The energy profiles shown in Figs. 2, 3, and 4 evidence that the present symmetric HAT proceeds across barrier heights of several kcal mol^{-1}. This means, as it is well known, that tunneling transmission is instrumental for the accurate description of the reaction mechanism. In addition, the pre-

Table 5 Calculated equilibrium constants (K_{eq} in cm^3 $molecule^{-1}$) for the formation of the $(H_2O)_2$, $(H_2O)_3$; H_2O…HO, $(H_2O)_2$…HO, and $(H_2O)_3$…HO complexes at different temperatures

Reaction[a]	278 K	288 K	298 K	308 K
3	5.55×10^{-21}	4.60×10^{-21}	3.87×10^{-21}	3.30×10^{-21}
4	8.61×10^{-20}	5.06×10^{-20}	3.09×10^{-20}	1.95×10^{-20}
5	1.72×10^{-19}	1.05×10^{-19}	6.68×10^{-20}	4.37×10^{-20}
6	9.75×10^{-21}	7.61×10^{-21}	6.05×10^{-21}	4.89×10^{-21}
7	8.87×10^{-21}	5.41×10^{-21}	3.40×10^{-21}	2.21×10^{-21}
8	6.83×10^{-19}	3.84×10^{-19}	2.24×10^{-19}	1.36×10^{-19}

[a] For the reaction see text

Table 6 Estimated tropospheric concentrations (in molecule cm^{-3}) of the $(H_2O)_2$, $(H_2O)_3$, H_2O…HO, $(H_2O)_2$…HO, and $(H_2O)_3$…HO complexes at different relative humidities (RH) and temperatures (T)

T	RH = 25%			RH = 50%			RH = 75%		
	H_2O	$(H_2O)_2$	$(H_2O)_3$	H_2O	$(H_2O)_2$	$(H_2O)_3$	H_2O	$(H_2O)_2$	$(H_2O)_3$
278	1.04×10^{17}	5.95×10^{13}	1.59×10^{12}	2.07×10^{17}	2.38×10^{14}	1.27×10^{13}	3.11×10^{17}	5.36×10^{14}	4.30×10^{13}
288	1.92×10^{17}	1.70×10^{14}	5.08×10^{12}	3.84×10^{17}	6.79×10^{14}	4.06×10^{13}	5.76×10^{17}	1.53×10^{15}	1.37×10^{14}
298	3.48×10^{17}	4.68×10^{14}	1.59×10^{13}	6.95×10^{17}	1.87×10^{15}	1.27×10^{14}	1.04×10^{18}	4.21×10^{15}	4.29×10^{14}
308	5.99×10^{17}	1.18×10^{15}	4.47×10^{13}	1.20×10^{18}	4.73×10^{15}	3.58×10^{14}	1.80×10^{18}	1.06×10^{16}	1.21×10^{15}
	H_2O…HO	$(H_2O)_2$…HO	$(H_2O)_3$…HO	H_2O…HO	$(H_2O)_2$…HO	$(H_2O)_3$…HO	H_2O…HO	$(H_2O)_2$…HO	$(H_2O)_3$…HO
278	1.01×10^{4}	9.28	7.24	2.02×10^{4}	3.71×10^{1}	5.79×10^{1}	3.03×10^{4}	8.35×10^{1}	1.96×10^{2}
288	1.46×10^{4}	1.52×10^{1}	1.32×10^{1}	2.92×10^{4}	6.08×10^{1}	1.05×10^{2}	4.39×10^{4}	1.37×10^{2}	3.55×10^{2}
298	2.10×10^{4}	2.49×10^{1}	2.44×10^{1}	4.21×10^{4}	9.95×10^{1}	1.95×10^{2}	6.31×10^{4}	2.24×10^{2}	6.58×10^{2}
308	2.93×10^{4}	3.87×10^{1}	4.21×10^{2}	5.85×10^{4}	1.55×10^{2}	3.36×10^{2}	8.78×10^{4}	3.48×10^{2}	1.14×10^{3}

These estimations have been done according Eqs. 3–8

The concentration of the hydroxyl radical employed for the formation of the $(H_2O)_n$…HO complexes is 1.0×10^{7} molecules cm^{-3}

reactive complexes also play a determining role in the form of interferences (resonances) that may be reflected in the transmission factor.

Quantifying the above tunneling, resonance features requires performing some sort of quantum dynamics study. The present systems involve a large number of coupled degrees of freedom, so that solving exactly the nuclear dynamics problem proves as a daunting task. To alleviate this problem, some of the authors recently developed a quantum dynamics methodology, based on restricting the molecular motion to the reaction path, so that the computational requirements are reduced to a minimal amount. Specific details of the methodology are given elsewhere [59]. Here, it suffices to understand that a properly defined wavepacket has been time evolved along the reaction profile, as provided by the reaction path, and the energy-dependent transmission factor is computed afterward, by means of a suitable Fourier transform of a reactants autocorrelation function. Results of the tunneling dynamics are shown below, restricted to one- and two-water cases, for the sake of deeming clearer the ensuing comparisons. Since in all the cases, the HAT mechanism is energetically favored (see Figs. 2, 3, 4), we limited ourselves to it. This process has proven to have an important tunneling contribution for reaction 1 as it has been pointed out in previous studies of the literature [19, 21].

Figure 5 shows the energy-dependent transmission factor, for the reaction between OH radical and one water molecule. Fixed-mass calculations are compared with variable mass, since this comparison provides interesting clues on the role played by perpendicular modes in the reaction dynamics. Fixed-mass calculations show an important tunneling contribution to transmission, as well as antitunneling at energies above the barrier. These are

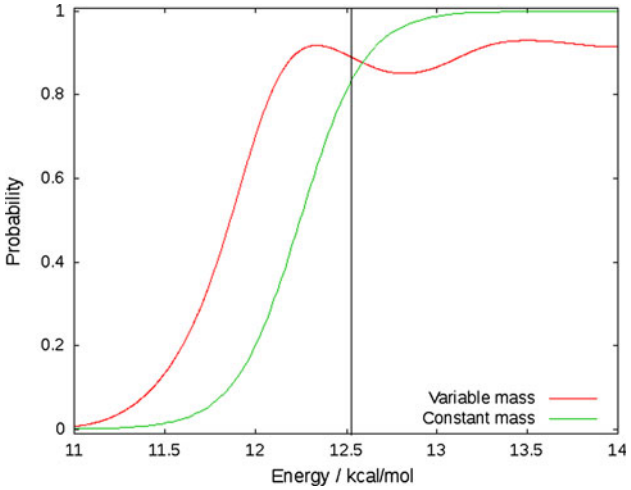

Fig. 5 Calculated transmission factor for the reaction between HO and H_2O. The *vertical black line* corresponds to the classical energy barrier

rather expected results, considering the fact that, in the present process, a light atom, hydrogen, is transmitted between two heavy centers (H_2O and O). In addition, inspection of the potential energy profile along the IRC clearly tells that one should expect tunneling to be important, since the barrier develops a rather thin profile, becoming thinner as energy is increased. This has been done by considering the geometries and frequencies obtained at BH&HLYP/6-311 + G(2df,2p) level of theory and the energies computed at CCSD(T)/aug-cc-pVTZ level of theory. However, tunneling appears even more enhanced, when one considers variable–mass results. One might then say that the influence of perpendicular modes is, rather surprisingly, to enhance reactivity below the

potential energy barrier. This is in contrast to numerous previous studies on tunneling, where the inclusion of more degrees of freedom normally inhibits tunneling. In addition, oscillations in the transmission factor, as energy is increased, are more intense in the variable–mass case, indicating that interference phenomena are enhanced by the inclusion of perpendicular modes. This is a suggestive result, whose origin may be traced back to the symmetric character of the present reactions and their Heavy–Light–Heavy nature.

Tunneling contribution to reaction, for the reaction between OH and two water molecules, is analyzed in Fig. 6. Q–RPH transmission factor, as a function of energy, is shown for *cis* and *trans* configurations of the water dimer. Results show, first, that *cis–trans* differences are only an energy shift, the qualitative shape being fairly equal. This is the reason why we do not show results for all the isomers in all cases, limiting ourselves to this case. Second, the contribution to tunneling is again remarkable, but the most outstanding feature is the oscillating nature of the transmission factor in the threshold and post-threshold regions. These oscillations are much more pronounced than the previous case. It is clearly an influence of the deeper **CR1** well (ca. 7.5 kcal mol^{-1} for the two-water case, versus ca. 3.8 kcal mol^{-1} well depth for the one-water reaction).

Further comparison between one- and two-water reactions evidences that, whereas tunneling is of similar importance for both reactions, antitunneling is remarkably larger in the one-water case. It is shown by the slower trend to unity, in the large energy regime, when comparing Figs. 5 and 6. This feature is interesting, since this large

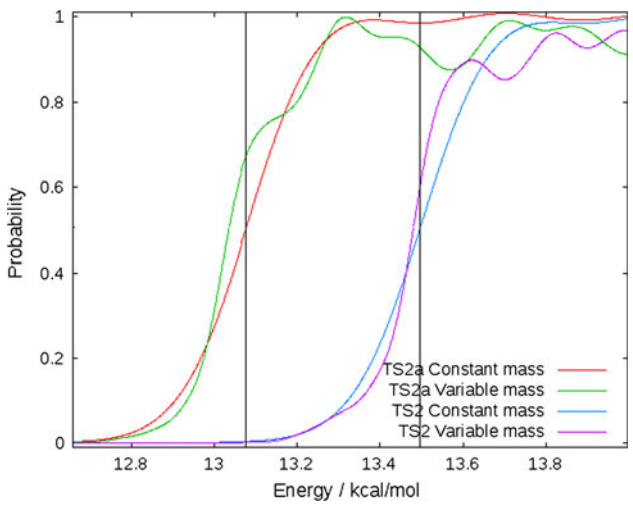

Fig. 6 Calculated transmission factor through **TS2** and **TS2a** for the reaction between HO and $(H_2O)_2$. The vertical black lines correspond to the classical energy barriers

antitunneling appears only in the variable mass case of the one-water reaction, *i.e.,* only when the perpendicular modes to reaction are taken into account. The primary conclusion is then that energy sequestering (from that available to reaction) is more effective for one-water than for two-water reactions. The explanation for such behavior might resort to a kind of entropic effect: energy flow concentrates more easily in a small number of non-reacting modes than in a larger number of them. In addition, the higher symmetry content, of the two-water TS, also suggests a much higher difficulty in concentrating the energy flow in non-reacting modes, when compared to the one-water reaction.

Once analyzed the behavior of the transmission factor along the reaction path, we computed the rate constant of the reaction. To do this, we considered the reactions to occur at 1 atm. of pressure, and we applied the steady-state approximation to the pre-reactive complex, and the rate constant is given by Eq. 9.

$$k_{TOT} = K_{eq} \cdot k_2 \cdot \kappa_{tun} \tag{9}$$

where K_{eq} is the equilibrium constant, k_2 is the unimolecular rate constant, and κ_{tun} is the tunneling contribution that has been computed by Eq. 10.

$$\kappa_{tun}(T) = \frac{\int_0^\infty T(E) \exp\left(-\frac{E}{k_B T}\right) dE}{\int_{V_b}^\infty \exp\left(-\frac{E}{k_B T}\right) dE} \tag{10}$$

We have to mention here that applying Eq. 9 is just a limiting case, and the effect of low pressures would require a different treatment that is beyond the scope of the present work.

In Table 7, we collected the computed rate constant. For the $H_2O + HO$ reaction, our computed values range between 2.76×10^{-17} and 6.04×10^{-17} cm^3 $molecule^{-1}$ s^{-1} in the 200–400 K range of temperatures and compare very well with the results reported by Masgrau et al. [19] and Uchimaru et al. [21], the differences with the last one being mainly attributed to the fact that they use a reaction profile beginning in the reactants without taking into account the pre-reactive complex. It is worth noting here the importance of the tunneling contribution, mainly at low temperatures, as it was pointed out in previous works on this reaction [19, 21].

Although for the case of the reaction between HO and $(H_2O)_2$ we report rate constants, we pointed out in a previous section that the pre-reactive complex **CR2** dissociates into $H_2O\ldots HO + H_2O$ and therefore, we can conclude that the reaction through **TS2** would not occur at all.

The reaction between hydroxyl radical and water trimer is much more complex, and k_2 is computed using Eq. 11 according to the unified statistical model [77], and the

Table 7 Computed rate constants for the reaction between hydroxyl radical and water, water dimer, and water trimer

Reaction OH + H_2O				
Temperature	K_{eq}	k_{TS1}	τ_{tun}	K_{TOT}
200	1.72×10^{-19}	5.09×10^{-6}	3.15×10^{7}	2.76×10^{-17}
250	2.19×10^{-20}	1.32×10^{-2}	5.33×10^{4}	1.54×10^{-17}
298	6.05×10^{-21}	2.04	1.40×10^{3}	1.73×10^{-17}
350	2.32×10^{-21}	9.92×10	1.28×10^{2}	2.95×10^{-17}
400	1.21×10^{-21}	1.58×10^{3}	3.16×10^{1}	6.04×10^{-17}
Reaction OH + $(H_2O)_2$				
Temperature	K_{eq}	k_{TS2}	τ_{tun}	K_{TOT}
200	1.90×10^{-17}	2.24×10^{-4}	1.05×10^{7}	4.47×10^{-14}
250	2.59×10^{-19}	4.04×10^{-1}	2.78×10^{4}	2.91×10^{-15}
298	1.57×10^{-20}	4.98×10	9.47×10^{2}	7.40×10^{-16}
350	1.77×10^{-21}	2.05×10^{3}	1.02×10^{2}	3.70×10^{-16}
400	3.70×10^{-22}	2.9×10^{4}	2.76×10	2.97×10^{-16}
Reaction OH + $(H_2O)_3$				
Temperature	K_{eq}	k_{TS5}	k_{TS6}	τ^{a}_{tun}	K_{TOT}
200	4.50×10^{-16}	6.14×10^{11}	1.24×10^{-5}	2.24×10^{7}	1.25×10^{-13}
250	4.40×10^{-18}	1.20×10^{12}	3.89×10^{-2}	4.01×10^{4}	6.86×10^{-15}
298	2.24×10^{-19}	1.89×10^{12}	6.95	1.11×10^{3}	1.73×10^{-15}
350	2.27×10^{-20}	2.73×10^{12}	3.83×10^{2}	1.08×10^{2}	9.37×10^{-16}
400	4.45×10^{-21}	3.56×10^{12}	6.76×10^{3}	2.77×10	8.33×10^{-16}

K_{eq} are in cm^3 $molecule^{-1}$, K_2 are in s^{-1}, then total constants K_{TOT} are in cm^3 $molecule^{-1}$ s^{-1}

τ_{tun} is the tunneling correction

K_2 stands for k_{TS1}, k_{TS2}, k_{TS5}, and k_{TS6}, respectively

[a] τ_{tun} applies to reaction through k_{TS6}

$$\frac{1}{k_2} = \frac{1}{k_{TS5}} + \frac{1}{k_{TS6}} \quad (11)$$

results displayed in Table 5 show that in this case, the reaction is much faster than reaction 1, with values ranging between 1.25×10^{-13} and 8.33×10^{-16} cm^3 $molecule^{-1}$ s^{-1} in the 200–400 K range of temperatures. Here, it is important to note that the tunneling contribution is very similar to those occurring in reaction 1.

4 Conclusions

The reactions between HO and $(H_2O)_n$ ($n = 1, 3$) have been investigated using high-level theoretical methods, and the results obtained allow us to highlight the following points.

Regarding the water dimer and trimer, our calculations predict a binding energy of 2.86 kcal mol^{-1} for $(H_2O)_2$ relative to $H_2O + H_2O$ and 7.67 kcal mol^{-1} for $(H_2O)_3$ relative to $(H_2O)_2 + H_2O$.

Our calculations predict atmospheric concentration for the $(H_2O)_2$ complex in the range between 5.95×10^{13} and 1.06×10^{16} molecule cm^{-3} and for the $(H_2O)_3$ complex in the range between 1.59×10^{12} and 1.21×10^{15} molecule cm^{-3}; depending on the atmospheric conditions of relative humidity and temperature. For the H_2O…HO complex, we predict atmospheric concentrations in the $1.01 \times 10^{4} - 8.78 \times 10^{4}$ molecule cm^{-3}, depending on the atmospheric conditions and considering a hydroxyl radical population of 10^7 molecule cm^{-3}. The concentration of the (H2O)$_2$…HO and $(HO)_3$…HO is predicted to be about two orders of magnitude smaller.

All the reactions considered are symmetric, and they begin with the formation of a pre-reactive hydrogen-bonded complex.

For the reaction of hydroxyl radical with a single water molecule, our calculations predict that the pre-reactive hydrogen-bonded complex **CR1** has a binding energy of 3.78 kcal mol^{-1}, whereas the transition state lies 12.53 kcal mol^{-1} above **CR1**. Very interestingly, we found a VRI point along the reaction path, which is energetically located close to 4 kcal mol^{-1} below the transition state, which allows branching the reaction path. The computed rate constant for this reaction range between 2.76×10^{-17} and 6.04×10^{-17} cm^3 $molecule^{-1}$ s^{-1} in the 200–400 K range of temperatures.

For the reaction between hydroxyl radical and water dimer, our calculations predict the pre-reactive complexes (**CR2** and **CR2a**) to have binding energies close to 7.5 kcal mol^{-1}. Then, the reaction can proceed in two different ways: (a) dissociating directly into the H_2O…HO

complex and H_2O, requiring an energy of ca 6.6 kcal mol^{-1} and (b) proceeding through three different elementary reactions. In this case, the more favorable path occurs through **TS2a**, which is predicted to lie 13.07 kcal mol^{-1} above **CR2a,** and it involves a hydrogen atom transfer mechanism. The high energy barrier computed for **TS2a** along with the rate constant computed for this elementary reaction indicated that the reaction between HO and $(H_2O)_2$ will produce H_2O…HO and H_2O, and it will contribute to the atmospheric formation of hydrated hydroxyl radical, which has an important significance in the chemistry of the atmosphere.

The reaction with hydroxyl radical and water trimer begins with the addition of the HO radical to the three-membered ring of the water trimer forming the **CR3** complex. Then, it occurs a geometrical rearrangement to form the four-membered ring **CR4** complex, which is computed to be 8.57 kcal mol^{-1} more stable than the reactants. Then, the reaction can go on through three different reactions paths. The more favorable one occurs through **TS6**, which is predicted to lie 5.27 kcal mol^{-1} above the separate reactants, and it involves a hydrogen atom transfer mechanism. This reaction is predicted to be faster than the reaction between hydroxyl radical and one water molecule, which has a rate constant in the range $1.25 \times 10^{-13} - 8.33 \times 10^{-16}$ cm^3 $molecule^{-1}$ s^{-1} in the 200–400 K range of temperatures, a fact that is attributed to the complexity of the whole reaction path.

For all the reactions considered, the transmission via tunneling effect is found to be very important, especially at low temperatures. Other features that also appear to be relevant from a dynamical point of view and that deserve more studies are the enhancement of tunneling due to the inclusion of perpendicular modes via the Q-RPH, the remarkable antitunneling for the reaction between HO and H_2O, and the oscillations in the transmission factor for the reaction of the HO radical and $(H_2O)_2$. The latter is attributed to an increment of resonances due to the deeper well of the corresponding **CR1** compared with the HO + H_2O case.

Acknowledgments This research has been supported by the Generalitat de Catalunya (Grant 2009SGR01472) and the Spanish Dirección General de Investigación Científica y Técnica (DGYCIT, grants CTQ2008-06536/BQU and CTQ2008-02856/BQU). The calculations described in this work were carried out at the Centre de Supercomputació de Catalunya (CESCA), at the Computational Center of CTI–CSIC, and at the cluster of workstations of our group. Antoni Aguilar-Mogas and Marc Caballero gratefully thank to Ministerio de Ciencia e Innovación for a predoctoral fellowship. Javier González and Miquel Torrent-Sucarrat acknowledge CSIC for a JAE-DOC contract.

References

1. Wayne RP (2000) Chemistry of atmospheres, 3rd edn. Oxford University Press, Oxford
2. Wennberg PO, Hanisco TF, Jaeglé L, Jacob DJ, Hintsa EJ, Lanzendorf EJ, Anderson JG, Gao RS, Keim ER, Donnelly SG, Negro LAD, Fahey DW, McKeen SA, Salawitch RJ, Webster CR, May RD, Herman RL, Proffitt MH, Margitan JJ, Atlas EL, Schauffler SM, Flocke F, McElroy CT, Bui TP (1998) Science 279:49–53
3. Monks PS (2005) Gas-phase radical chemistry in the troposphere. Chem Soc Rev 34:376–395
4. Jaeglé L, Jacob DJ, Brune WH, Wennberg PO (2001) Atmos Environ 35:469–489
5. Hofzumahaus A, Rohrer F, Lu KD, Bohn B, Brauers T, Chang CC, Fuchs H, Holland F, Kita K, Kondo Y, Li X, Lou SR, Shao M, Zeng LM, Wahner A, Zhang YH (2009) Science 324(5935):1702–1704. doi:10.1126/science.1164566
6. Mansergas A, Anglada JM (2007) ChemPhysChem 8:1534–1539
7. Jacob DJ (2000) Atmos Environ 34(12–14):2131–2159
8. Chameides WL, Davis DD (1982) J Geophys Res Oceans Atmospheres 87(NC7):4863–4877
9. Hanson DR, Burkholder JB, Howard CJ, Ravishankara AR (1992) J Phys Chem 96(12):4979–4985
10. Kregel KC, Zhang HJ (2007) Am J Physiol Regul Integr Comp Physiol 292(1):R18–R36
11. Pryor WA, Houk KN, Foote CS, Fukuto JM, Ignarro LJ, Squadrito GL, Davies KJ (2006) Am J Physiol Regul Integr Comp Physiol 291(3):R491–R511
12. Fridovich I (1998) J Exp Biol 201(Pt 8):1203–1209
13. Kehrer JP (2000) Toxicology 149(1):43–50
14. Cooper WJ, Cramer CJ, Martin NH, Mezyk SP, O'Shea KE, von Sonntag C (2009) Chem Rev 109(3):1302–1345. doi:10.1021/cr078024c
15. Sein MM, Golloch A, Schmidt TC, von Sonntag C (2007) ChemPhysChem 8(14):2065–2067
16. Lesko TM, Colussi AJ, Hoffmann MR (2004) J Am Chem Soc 126:4432–4436
17. Sehested K, Corfitzen H, Holcman J, Hart EJ (1998) J Phys Chem A 102:2667–2672
18. Dubey MK, Mohrschladt R, Donahue NM, Anderson JG (1997) J Phys Chem A 101(8):1494–1500
19. Masgrau L, Gonzalez-Lafont A, Lluch JM (1999) J Phys Chem A 103(8):1044–1053
20. Masgrau L, Gonzalez-Lafont A, Lluch JM (1999) J Comput Chem 20(16):1685–1692
21. Uchimaru T, Chandra AK, Tsuzuki S, Sugie M, Sekiya A (2003) J Comput Chem 24:1538–1548
22. Hand MR, Rodriquez CF, Williams IH, Balint-Kurti GG (1998) J Phys Chem A 102(29):5958–5966
23. Basch H, Hoz S (1997) J Phys Chem A 101(24):4416–4431
24. Deyerl HJ, Luong AK, Clements TG, Continetti RE (2000) Faraday Discuss 115:147–160
25. Olivella S, Anglada JM, Sole A, Bofill JM (2004) Chem Eur J 10:3404–3410. doi:10.1002/chem.200305714
26. Vohringer-Martinez E, Hansmann B, Hernandez H, Francisco JS, Troe J, Abel B (2007) Science 315(5811):497–501
27. Anglada JM, Gonzalez J (2009) ChemPhysChem 10(17):3034–3045. doi:10.1002/cphc.200900387
28. Luo Y, Maeda S, Ohno K (2009) Chem Phys Lett 469:57–61
29. Aloisio S, Francisco JS, Friedl RR (2000) J Phys Chem A 104:6597–6601

30. Zhu RS, Lin MC (2002) Chem Phys Lett 354(3–4):217–226
31. Anglada JM, Aplincourt P, Bofill JM, Cremer D (2002) ChemPhysChem 2:215–221
32. Crehuet R, Anglada JM, Bofill JM (2001) Chem Eur J 7(10):2227–2235
33. Neeb P, Sauer F, Horie O, Moortgat GK (1997) Atmos Environ 31(10):1417–1423
34. Gonzalez J, Torrent-Sucarrat M, Anglada JM (2010) PhysChemChemPhys 12(9):2116–2125. doi:10.1039/b916659a
35. Bahnson BJ, Colby TD, Chin JK, Goldstein BM, Klinman JP (1997) Proc Natl Acad Sci USA 94(24):12797–12802
36. Giese K, Petkovic M, Naundorf H, Kuhn O (2006) Phys Rep Rev Sect Phys Lett 430(4):211–276. doi:10.1016/j.physrep.2006.04.005
37. Guallar V, Gherman BF, Miller WH, Lippard SJ, Friesner RA (2002) J Am Chem Soc 124(13):3377–3384. doi:10.1021/ja0167248
38. Makri N (1999) Annual Rev Phys Chem 50:167–191
39. Pfeilsticker K, Lotter A, Peters C, Bosch H (2003) Science 300(5628):2078–2080
40. Dunn ME, Pokon EK, Shields GC (2004) J Am Chem Soc 126:2647–2653
41. Goldman N, Fellers RS, Leforestier C, Saykally RJ (2001) J Phys Chem A 105(3):515–519
42. Becke AD (1993) J Chem Phys 98:1372
43. Frisch MJ, Pople JA, Binkley JS (1984) J Chem Phys 80:3265–3269
44. Hehre WJ, Radom L, Schleyer PvR, Pople JA (1986) Ab initio molecular orbital theory. Wiley, New York, pp 86–87
45. Ishida K, Morokuma K, Kormornicki A (1977) J Chem Phys 66:2153
46. Gonzalez C, Schlegel HB (1989) J Chem Phys 90:2154
47. Gonzalez C, Schlegel HB (1990) J Phys Chem 94:5523
48. Fukui K (1970) J Phys Chem 74(23):4161
49. Cizek J (1969) Adv Chem Phys 14:35
50. Barlett RJ (1989) J Phys Chem 93:1963
51. Pople JA, Krishnan R, Schlegel HB, Binkley JS (1978) Int J Quant Chem XIV:545–560
52. Pople JA, Head-Gordon M, Raghavachari K (1989) J Chem Phys 90(8):4635–4636
53. Dunning THJ (1989) J Chem Phys 90:1007
54. Kendall RA, Dunning TH, Harrison RJ (1992) J Chem Phys 96(9):6796–6806
55. Pople JA, Head-Gordon M, Raghavachari K (1987) J Chem Phys 87:5968
56. Roos BO (1987) Adv Chem Phys 69:399
57. Frisch MJ, Trucks GW, Schlegel HB, Scuseria GE, Robb MA, Cheeseman JA Jr, Montgomery J, Vreven T, Kudin KN, Burant JC, Millam JM, Iyengar SS, Tomasi J, Barone V, Mennucci B, Cossi M, Scalmani G, Rega N, Petersson GA, Nakatsuji H, Hada M, Ehara M, Toyota K, Fukuda R, Hasegawa J, Ishida M, Nakajima T, Honda Y, Kitao O, Nakai H, Klene M, Li X, Knox JE, Hratchian HP, Cross JB, Adamo C, Jaramillo J, Gomperts R, Stratmann RE, Yazyev O, Austin AJ, Cammi R, Pomelli C, Ocherski JW, Ayala PY, Morokuma K, Voth GA, Salvador P, Dannenberg JJ, Zakrzewski VG, Dapprich S, Daniels AD, Strain MC, Farkas O, Malick DK, Rabuck AD, Raghavachari K, Foresman JB, Ortiz JV, Cui Q, Baboul AG, Clifford S, Cioslowski J, Stefanov BB, Liu G, Liashenko A, Piskorz P, Komaromi I, Martin RL, Fox DJ, Keith T, Al-Laham MA, Peng CY, Nanayakkara A, Challacombe M, Gill PMW, Johnson B, Chen W, Wong MW, Gonzalez C, Pople JA (2004) Gaussian 03, revision C.01 edn. Gaussian, Inc., Wallingford, CT
58. Schmidt MW, Baldridge KK, Boatz JA, Elbert ST, Gordon MS, Jensen JH, Koseki S, Matsunaga N, Nguyen KA, Su SJ, Windus TL, Dupuis M, Montgomery JA (1993) Gamess 2004. J Comput Chem 14:1347–1363
59. Gonzalez J, Gimenez X, Bofill JM (2009) J Chem Phys 131(5):054108. doi:10.1063/1.3194135
60. Gonzalez J, Gimenez X, Bofill JM (2001) J Phys Chem A 105(20):5022–5029. doi:10.1021/jp003793k
61. Gonzalez J, Gimenez X, Bofill JM (2007) J Comput Chem 28(13):2111–2121. doi:10.1002/jcc.20729
62. Gonzalez J, Gimenez X, Bofill JM (2007) J Comput Chem 28(13):2102–2110. doi:10.1002/jcc.20728
63. Gonzalez J, Gimenez X, Bofill JM (2004) Theor Chem Acc 112(2):75–83. doi:10.1007/s00214-004-0571-6
64. Askar A, Cakmak AS (1978) J Chem Phys 68(6):2794–2798
65. Klopper W, de Rijdt J, van Duijneveldt FB (2000) PhysChemChemPhys 2(10):2227–2234
66. Zhou Z, Qu Y, Fu A, Du B, He F, Gao H (2002) Int J Quant Chem 89:550–558
67. Cooper PD, Kjaergaard HG, Langford VS, McKinley AJ, Quickenden TI, Schofield DP (2003) J Am Chem Soc 125(20):6048–6049
68. Engdahl A, Karlstrom G, Nelander B (2003) J Chem Phys 118(17):7797–7802
69. Ohshima Y, Sato K, Sumiyoshi Y, Endo Y (2005) J Am Chem Soc 127(4):1108–1109
70. Allodi MA, Dunn ME, Livada J, Kirschner KN, Shields GC (2006) J Phys Chem A 110(49):13283–13289
71. Soloveichik P, O'Donnell BA, Lester MI, Francisco JS, McCoy AB (2010) J Phys Chem A 114(3):1529–1538. doi:10.1021/jp907885d
72. Quapp W, Hirsch M, Heidrich D (1998) Theor Chem Acc 100(5–6):285–299
73. Ess DH, Wheeler SE, Iafe RG, Xu L, Celebi-Olcum N, Houk KN (2008) Angew Chem Int Ed Engl 47(40):7592–7601. doi:10.1002/anie.200800918
74. Valtazanos P, Ruedenberg K (1986) Theor Chim Acta 69(4):281–307
75. Tsuji K, Shibuya K (2009) J Phys Chem A 113(37):9945–9951. doi:10.1021/jp903648z
76. Anglada JM (2004) J Am Chem Soc 126(31):9809–9820
77. Miller WH (1976) J Chem Phys 65:2216–2223